Interaction mechanisms among waves, currents and a submerged plate

Interaction mechanisms among waves, currents and a submerged plate

Dezhi Ning[1], Lifen Chen[1, 3*], Hongxing Lin[1], Qingping Zou[1, 2], Bin Teng[1]

1. State Key Laboratory of Coastal and Offshore Engineering, Dalian Univ. of Technology, Dalian 116024, China; Email: lifen.chen@uwa.edu.au; chenlifen239@163.com.
2. The Lyell Centre for Earth and Marine Science and Technology, Institute for Infrastructure and Environment, Heriot-Watt University, Edinburgh, EH14 4AS, UK.
3. Oceans Graduate School, Faculty of Engineering and Mathematical Sciences, University of Western Australia, Crawley, WA, 6009, Australia.

ABSTRACT

Wave-induced loads on a submerged plate, representative of submerged breakwater, coastal-bridge deck and a certain type of wave energy converter, in a uniform current are investigated in this study using fully nonlinear NWTs (numerical wave tanks) based on potential flow theory. The coupling effect of wave and current is explored, and the underlying interaction mechanisms of the hydrodynamic forces are described. The presence of a background current modifies the frequency dispersion. It produces changes of the water-surface elevation, and also has an effect on wave-induced loads. Depending on the nonlinearity, higher harmonic wave components are generated above the submerged plate. These contribute to the wave forces. It is found that the horizontal and the vertical force, hence the moment, are affected in opposite way by the currents. The Doppler shifted effect dominates the vertical force and the moment on the plate. Whereas, the Doppler shifted effect and the generation of higher harmonics play opposite roles on the horizontal forces. The contribution of 2nd order harmonics is up to 30% of the linear component. The current-induced drag force, represented by the advection term $\rho U\partial\phi/\partial x$ in the pressure equation, is found to lead to a decrease in the moment for the most range of wavelengths considered, and an increase for a small range of longer waves.

KEYWORDS: fully nonlinear numerical wave tanks; combined wave-current flow; submerged flat plate; wave forces and moment; current-induced drag force; higher harmonic waves.

1. INTRODUCTION

The cost-effective and safe design of a submerged breakwater, one of the most important types of coastal protection structures, requires a better understanding of the destructive loads acting on such structure. The coastal submerged breakwater is usually in the form of horizontal plate. A submerged horizontal plate breakwater has an advantage that it is less dependent on the foundation conditions when compared to traditional, for example, impermeable slope breakwater [1]. Foundation stability is usually required for traditional impermeable breakwaters [2-3, 66-67].

A submerged horizontal plate is also widely used to represent coastal bridge deck that may be fully inundated by storm surges, and the submerged wave energy converter (WEC) plate. The calculation of forces even on fixed submerged WEC plates is essential and is a step towards considering the wave-induced motions of WECs.

The wave-induced loads on a submerged horizontal plate can be estimated by (1) semi-empirical formulae in which the total force is decomposed into different components. The force coefficient for each component is determined empirically based on physical and/or numerical experiments [4-9]; (2) pressure integration around the structure in which the wave pressure is calculated using different numerical tools including, but not limited to: diffraction analysis [10-14], numerical wave tanks (NWTs) based on potential flow theory [15-18], Computational Fluid Dynamics (CFD) simulations

*Corresponding author. Email:chenlifen239@163.com; lifen.chen@uwa.edu.au

[19-21] and the theory of Level I Green-Naghdi (GN) equations [21-24]. Diffraction analysis which solves the Laplace equation for fluid motions in frequency domain considers the nonlinear wave-structure interactions up to 2nd order. If nonlinearity higher than 2nd order is important, NWTs and CFD simulations should be used. The former solves the Laplace equation with fully nonlinear free surface conditions in time domain. The latter solves the full Navier-Stokes equations, hence, are able to capture all nonlinear effects involved and the viscous effect. Obviously, CFD simulations are computational more intensive and expensive when compared to diffraction analysis and NWTs. The Level I GN equations are applicable to the flow of long waves in shallow water due to its inherent assumptions. In the theory of Level I GN, the vertical velocity component varies linearly along the water depth while the horizontal velocity component remains unchanged along this direction. Nevertheless, the majority of studies on the subject have so far concentrated on the wave-only conditions.

However, in coastal areas where the submerged breakwaters are likely to be located, waves usually co-exist with currents that generated by tides, local and/or global circulation etc. Thus, the interaction of nonlinear waves propagating on a current with submerged horizontal plates has direct practical applications. Although current flows in some regions in the open sea may exhibit some degree of variation in the vertical direction [25-28, 68], the approximation of vertically-uniform current distribution is still useful. Obviously, it is mathematical easier to solve problems that involve wave-uniform current interactions. Lavrenov [29] stated that in shallow water, the effect of velocity shear on wave transformations is relatively small when compared to the effect of current itself. It is reasonable to describe the current flow using the surface velocity or the depth-averaged velocity only. Additionally, the knowledge on wave-uniform current interaction is helpful and important when/if the 'equivalent uniform current' is identified [30]. The coexistence of wave and opposing current may lead to the formation of large amplitude waves, i.e. rogue waves, with the amplitude being up to 3 times larger than the initial wave amplitude, see for example, Toffoli et al. [48-50], Onorato et al. [51] and Alberello et al. [52]. This would without doubt lead to huge destructive loads on the structures. We note here that the wave and current conditions considered in this work, however, do not excite any wave instability.

Much previous work on wave-uniform current-structure interaction has primarily concentrated on wave radiation and diffraction around the structure [31-34], or wave reflection and transmission characteristics if a submerged breakwater is considered [35-37]. Some of these studies may consider wave forces but were presented in a form to demonstrate that the proposed methods can be act as ad hoc approaches to calculate forces. A more thorough investigation is required to understand the underlying physics that would play significant role in determining wave and current forces on submerged horizontal plate.

This work investigates forces and moments on a submerged plate that is subject to the combined wave-current flows using NWTs. As discussed previously, the assumption inherent to NWT makes it incapable of capturing underlying physics associated with fluid viscosity if this is important. Rey et al. [33], Koo and Kim [38], Liu et al. [39], among others, indicated that the potential flow theory is adequate for wave-current-submerged structure interactions when the current velocity is smaller than 15% of the incident wave velocity. The maximum current velocity considered in this work is about 20% of the incident wave velocity. Although this percentage is slightly larger, the analysis followed shows that the NWTs still somehow work well within this range. The NWT is computational cheaper than CFD simulations, hence, a promising tool to model wave-uniform current-structure interactions. The rest of the paper is organized as follows. The details of the NWTs used are briefly summarized in Section 2. The NWT model is verified in Section 3 by comparing with published analytical results and experimental measurements. A series of parametric studies are carried out in Section 4 to study the sensitivity of wave-induced loads to the current velocity and the incident wave characteristics. The underlying interaction mechanisms that would affect the wave loading on the structure are also investigated in this section. Finally, conclusions are given in Section 5.

2. NUMERICAL WAVE TANK

Lin et al. [37] developed a NWT based on potential flow theory to investigate wave transmission and reflection from a submerged plate in the presence of constant currents. The generation of higher

harmonic waves due to shoaling effect above the submerged plate was considered. This NWT is extended in this study to estimate the forces and moment on a submerged horizontal plate in combined wave-current flows. The acceleration potential method is applied to calculate the hydrodynamic wave pressure, which are then integrated to get the total hydrodynamic wave forces and moment on the submerged plate. The underlying mathematical formulations and the numerical implementation are summarized briefly in the Appendixes 1-2. It is recommended to refer to Lin et al. [37] for more details.

Fig.1 shows the simplified sketch of the problem in two-dimension. The wave is generated from the left end of the NWT and approaches towards a submerged plate located in the centre of the numerical wave tank (NWT). Numerical beaches are implemented at both ends of the NWT to minimize the reflected waves from the structure and the right end of the NWT. Also shown in Fig.1 is the coordinate system used in this study. The x-axis is positive in the wave propagation direction with its origin at the left end of the tank, and the z-axis is positive upward with $z = 0$ at the mean free surface. h is the water depth. In theory, the NWTs are capable of simulating nonlinear waves in an arbitrary water depth, i.e. h can be an arbitrary value constraints to the breaking limit [58], though only shallow and intermediate water depths are considered in this work. It is also worth noting that the NWTs consider the nonlinearities arising from both the wave evolution and the wave-structure interactions in a depth-uniform current, though the latter may be more important for the cases considered in this work.

U is the velocity of a constant current propagating in parallel with the incoming wave. Positive and negative U mean that the current is in the same and opposite direction of the incoming wave, respectively. Terminologies co- and counter-current propagating waves are used in this paper to indicate the waves that propagate in the same and opposite direction as the current, respectively. And the corresponding currents are referred as wave-following and opposing currents, respectively.

The regular waves are characterized by the wave steepness kA and the relative water depth kh in which k is the wave number. The wave amplitude A can either be the one measured in the absence of a current or the one in currents, which are labelled as A_0 and A_e, respectively. These are calculated based on the free surface elevation time series measured in the absence of a structure, i.e. the undisturbed waves calculated using the NWTs. More specially, A_0 and A_e are the wave amplitudes of the corresponding linear components, obtained by applying the FFT analysis to the undisturbed wave signals.

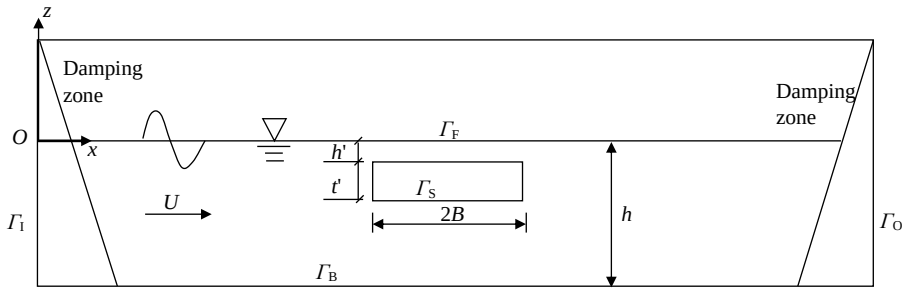

Fig. 1 Sketch of a 2-D numerical wave tank of wave-current-structure interactions.

2-D numerical wave tanks were set-up to replicate as closely as possible the theoretical and/or experimental set-ups presented in [12] and [35], and were extended to investigate the interaction mechanisms among waves, current and a submerged plate. The total length of the computational domain was ~13λ with a distance of ~4.5λ between the front damping zone (left damping zone as shown in Fig.1) and the structure to ensure full development of the incoming wave, and the combined wave-current flows before the complex interactions with the structure. λ is the wavelength of the incoming wave propagating in the absence of a current and the plate. Compared to the physical experiments, e.g. Lin et al. [37] and Chen et al. [54], the structure was rather close to the numerical wave paddle. Huseby and Grue [65] suggested to have a relatively long distance between the physical wave paddle and the structure to get a relatively long time window in which the spurious free second harmonic wave hasn't arrived and contaminated the results of concern yet. Nevertheless, the detailed comparisons between

the numerical results and the experimental measurements (e.g. Fig.3, [37]) indicate that the use of a relative short numerical wave flume is somehow appropriate to improve the computational efficiency, while still maintaining the correct wave-wave and wave-current evolutions, as well as the flow field around the structure. Similar treatments have been applied in e.g. Chen et al. [28, 55-58]. The first and last 2λ of the numerical wave tank were used as relaxation zones to minimize/avoid reflected waves from the structure and left output wall (right end of the wave tank, Fig.1). This enabled long simulations with a relative short numerical wave tank.

It is noted that we model waves on a uniform current by disturbing the original parallel uniform current, which is realized by specifying prescribed velocity potentials and free surface elevations at the input boundary faces, see the Appendix 1. The entrance effect of wave propagating into an opposing current is not simulated, and we leave this additional complication for future.

The mesh sizes of the computational domain were determined by convergence tests, which are not shown here for brevity. Details can be found in Lin et al; [37]. The optimum mesh size was determined with a horizontal grid size of $\lambda/30$ around the free surface, and the vertical grid size of $h/20$ at the inlet and outlet boundaries (left and right end of the wave flume). The time step was set at $T/40$ in which T is the wave period. In presence of the structure, a mesh size of $B/90 \times t'/2$ was used for discretizing the structure. B and t' are the half width and the thickness of the structure, respectively, see also Fig. 1.

3. VERIFICATION OF WAVE-INDUCED FORCES AND MOMENTS

In this section, the NWT is firstly applied to estimate the wave-induced forces and moment on a submerged structure in the absence of a current, i.e. in initial still water, and the predictions for waves propagating in depth-uniform currents are also provided. The numerical models are validated by comparing with both linear wave theory and published experimental measurements. It is noted that the incoming wave considered in this work has a wave steepness ranging from small, nearly linear waves, to very large, nearly breaking waves. The combined hydrodynamics due to co-existing wave and current is explored. The detailed studies associated with the combined wave-current flow fields, local wave fields and the reflection and transmission characteristics have been presented in e.g. Lin et al. [37] and Chen et al. [54, 56], hence omitted here for brevity.

3.1 Wave-induced linear forces and moment in the absence of a current

The physical problem of a small linear wave propagating over an infinitely long submerged plate in the absence of a current is considered firstly. The results from the proposed NWT are compared with the linear FEM (finite element method) and the LWA (long wave approximation) solutions described in [12]. In accordance with linear wave theory, the wave amplitude $A_0 = 0.005$ m and the wave period $T = 12.64$ s in full scale are considered. This corresponds to a wavelength λ of 25 m. The submergence $h'/h = 0.3$, where the water depth above the submerged plate $h' = 0.12$ m; representation of the variables refers to Fig. 1.

The variation of horizontal and vertical forces on the submerged plate are plotted in Fig. 2 as a function of B/L'. The magnitude of the horizontal force is non-dimensional dividing by $\rho g A_0 t'$ and the vertical force by $\rho g A_0 B$ following those in [12]. L' is the wavelength above the submerged plate, and the representation of B and t' (= 0.1 m) can be found in Fig. 1. It is noted that the submergence h' is used for calculating the L', i.e. L' is different from λ defined above where the water depth h is used for calculation. It can be seen that the NWT model results are in a good agreement with the FEM and the LWA solutions although small phase shifts are observed. This could result from the inherent nonlinear interaction process and the generation of free waves, although they are expected to be small for this particular wave. These nonlinear effects involved are not considered by the linear FEM and the LWA solutions.

Both horizontal and vertical forces alternatively increase to the peak value and then decrease to zero at certain locations. The pressure on both edges of the plate is in phase with each other, thus, cancel each other at about $B/L' = 1$, which results in the zero horizontal force at this point. The behavior of the

vertical force is, however, determined by the combined effect of the periodic wave motion above the plate and the sloshing-like flow motion beneath the plate. The flow behaviors on both horizontal sides of the plate can be clearly observed in Fig. 3 in which the distribution of the maximum dynamic pressure on the upper and lower surfaces of the plate are plotted. The positive pressure under wave crest and the negative pressure under wave trough on the upper surface of the plate would cancel each other in the integration process. Clearly, the ratio, B/L', is thus a key parameter in characterizing the vertical wave force on the submerged plate because it determines the number of crests and troughs, as shown in Fig. 3. Patarapanich [12] associated the positions of zero forces with the positions of zero reflections.

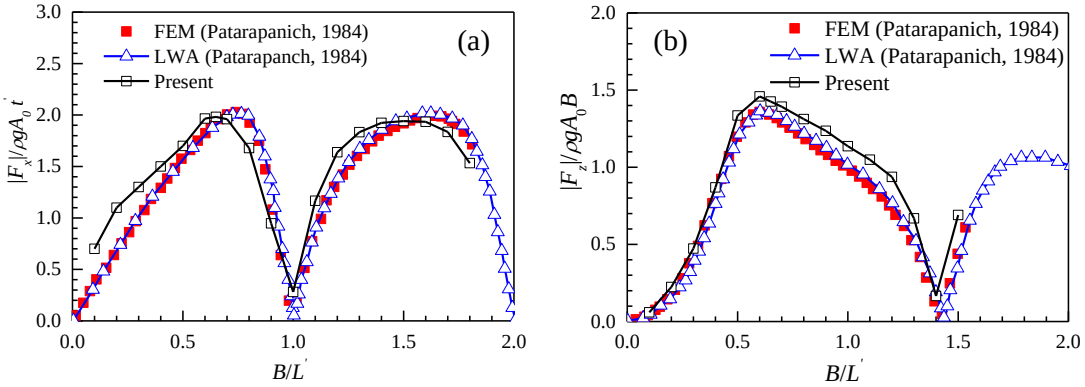

Fig. 2 Variation of the horizontal (a) and vertical (b) forces along the plate width for h'/h = 0.3, and h/L = 0.016.

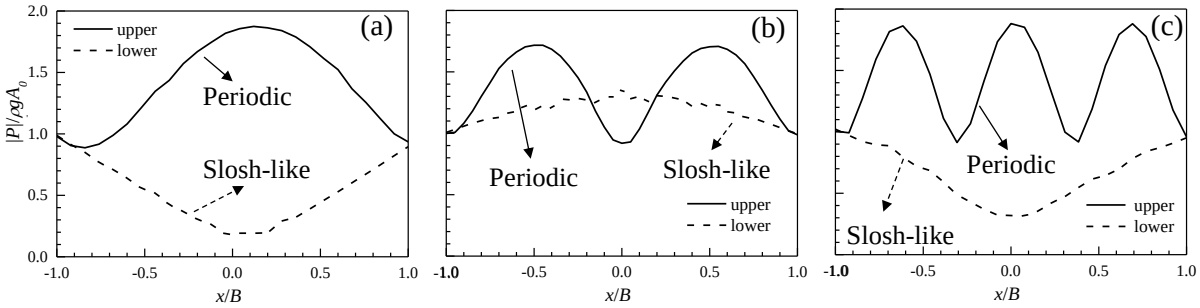

Fig. 3 Evolution of the maximum dynamic pressure P along the submerged plate for (a) B/L'=0.5; (b) B/L'=1.0; (c) B/L'=1.5.

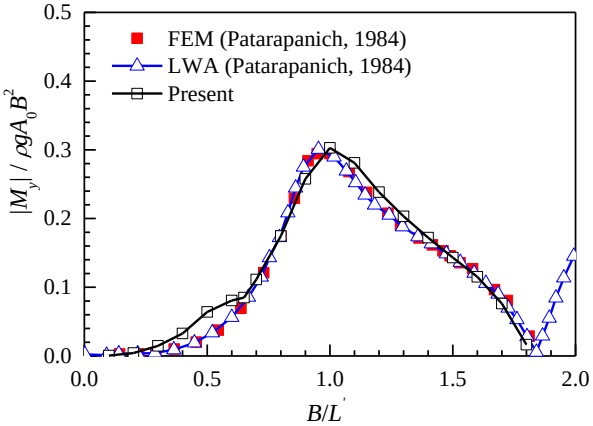

Fig. 4 Variation of the moment around the centre of the plate for h/h' = 0.3, and h/L = 0.016.

The overturning moment around the horizontal centre of the plate is shown in Fig. 4. The moment is non-dimensional dividing by $\rho g A_0 B^2$. B is used because for a thin plate, the vertical force on the plate is much larger than the horizontal force, thus, dominates the induced moment. The ratio of the latter and the former is about 2.5%. Similar to the forces, the moment increases to its peak value at about $B/L' = 1$ while decreases to zero at about $B/L' = 1.835$. The agreement between the NWT results and the FEM as well as LWA solutions is also favorable although slightly phase shifts among them are observed.

It is worth mentioning that flow over a submerged plate may show similar behaviours (to a certain level) to the phenomena so-called "overwash" and "greenwater", for example, the flow behaviours on the lower surface of the plate, and the shallow-water flows above the plate. Overwash refers to water overturning over the top of a plate in moderate waves [59-60], while water overturning in greenwater may occur as a result of the extreme wave-structure interactions in storm/cyclonic sea-states [57, 61]. The freeboard, i.e. the distance between the mean sea-level and the top surface of the structure, is negative (= the submergence h'), nearly zero, and positive, respectively, for the three phenomena aforementioned. Note that the ratio of the freeboard and the draft for greenwater usually ranges from 0.2 to 1 depending on the loading condition of the vessel.

3.2 Wave-induced forces and moment in presence of currents

Rey and Touboul [35] extended the work of Patarapanich [12], taking into account the effect of water currents that flow in the wave propagation direction. Experimental measurements were also provided for cross-checking the analytical and experimental models. In the experiments, $2B = 1.53$ m, $t' = 0.1$ m, $h = 3$ m, and $h' = 0.5$ m; detailed representation of these variables refers to Fig.1. Regular waves with a amplitude ranging from 0.03 to 0.22 m, and a depth-uniform current with velocity of 0.3 m/s (i.e. $U = +0.3$ m/s) were generated. The wave period ranged from 1.1 to 3.2 s. Thus, the wave steepness considered ranged from 0.02 to 0.2, covering the range of linear to very steep, nearly breaking waves, and the U/C_{g0} was in the range of (0.06 - 0.17). C_{g0} is the wave group velocity in the absence of a current.

Rey and Touboul [35] claimed that the partially reflected waves from the wave absorber observed in the experiments can be used to mimic the reflection from the shorelines or coastal structures being protected by submerged breakwaters. It was found that the tests considering wave-only conditions experienced significant reflected waves, while the wave absorber somehow worked better for the tests in presence of a following current. Analytical solutions calculated without and with the reflection from wave absorber were then considered in [35] to investigate the effect of wave reflections from the shore. The observation of weaker reflection in presence of a following current was further confirmed by the fact that the analytical solutions without the reflection being considered agreed better with the experimental results for wave-current cases.

Fig. 5 shows the variations of the force and moment against the wave number kh for cases with a following current. Both experimental and present NWT results are included. The wave number kh is used for the sake of comparison as this was used in [35]. It is noted that the current-affected amplitude A_e is now used for the normalization. Model 1 and Model 2 in Fig. 5 represent the analytical solutions in [35] that were calculated without and with the reflection from wave absorber, respectively. In Model 2, the reflection coefficients and phase shifts were parameterized by using the free surface elevations measured far downstream the plate and near the wave absorber, i.e. they were determined empirically, and the relevant information was not provided.

It can be seen from Figs. 5 (a-b) that both the horizontal and vertical forces increase with increasing kh to the maximum and then decrease with further increase of kh, though the locations of the maxima are different. An opposite trend (i.e. decreases first followed by an increase at larger kh) is found for the moment around the centre of the plate using the NWTs and the experiments, while the analytical solutions in [35] somehow failed to capture this trend. Additionally, a homogenized behaviour of the moment for larger kh (>5) is found in the presence of currents, meaning that the moment become less sensitive to the frequency for short waves.

In conclusion, the NWTs used in this work agree better with experimental measurements when compared to the analytical solutions presented in [35]. This could attribute to the fact that the NWT is able to consider fully nonlinear wave-current and wave-current-structure interactions. The deviations from the analytical solutions are relatively larger for a smaller kh (kh <5) in terms of horizontal forces and moments, and for a larger kh (kh >5) in terms of the vertical force. This indicates that the nonlinearity plays more significant role on the horizontal force and the moment with a longer wave, and vice versa for the vertical force.

A set of simulations in the absence of a current was also performed and the results, including the comparisons with the experiments, are presented in the Appendix 3. We note that the reflection from the outlet boundary of the tank was not considered/intended in the NWTs, hence, only qualitative comparisons with the experiments for wave-only cases (for which the wave reflections were significant) are carried out. The verification for wave-only cases has been carried out in Section 3.1 and in [62], and [63], among others.

Generally, the existence of a following current results in an increase (up to 30%) and a decrease in the horizontal and vertical forces, respectively. It is clearly that the horizontal, and the vertical force, hence the moment, are affected in opposite ways by the currents. This motivates the exploration on the underlying mechanisms associated with the determination of the global behaviours of the loads, including effects of the Doppler shift and the nonlinearities arising from both wave-current evolutions and wave-current-structure interactions. The effect of current on these underlying mechanisms may be different, and hence, results in the opposite trend.

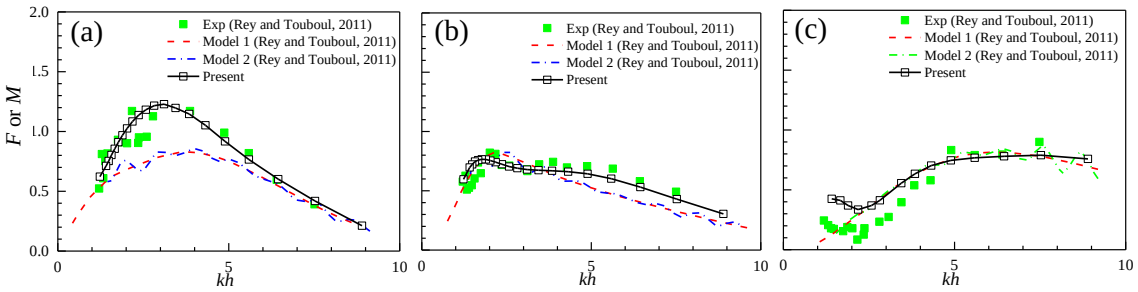

Fig. 5 Variations of the horizontal force $|F_x|/\rho g A_e t'$ (a), vertical force $|F_z|/\rho g A_e B$ (b), and moment $|M_y|/\rho g A_e B^2$ (c) with kh for combined wave-current cases with U = + 0.3 m/s. The moment is scaled up by a factor of 10.

4. NUMERICAL RESULTS AND ANALYSIS

In this section, the validated NWT models are used to investigate the interaction mechanisms involved. The well-recognized Doppler shifted effect is described first, followed by the discussion associated with the generation of higher harmonic free waves above the submerged plate. At last, the effect of the advection term, $\rho U \partial\phi/\partial x$, in the pressure equation (A8) is studied using NWTs. This term is named 'current-induced drag force' unless otherwise stated for brevity. This drag force cannot be easily isolated by physical model testing. The wave steepness considered ranged from 0.02 to 0.2, and the U/C_{g0} ranged from ~ (-0.2) to ~0.17.

4.1 Doppler shifted effect

The case of regular waves propagating over a depth-uniform current has been studied for decades, and it is well known that the combined water kinematics can be simply treated as a Doppler shifted solution in which the wave amplitude decreases and increases in a following and opposing current, respectively. The opposite trend is found in the wavelength. One would thus expect a decrease/increase in the consequent force and moment on the structure in a following/opposing current. This hypothesis

fails to describe the load behavior in terms of the horizontal force, as discussed previously in the last paragraph of Section 3.1.

Two sets of scales are introduced to study the effect of the increased/decreased wave amplitude on the wave loading, i.e. the Doppler effect for the wave loading. A_0 and A_e are used in the first and second set of scales, respectively. Recalling that A_0 is the wave amplitude measured/recorded in the absence of a current while A_e is the current-affected wave amplitude, i.e. this wave amplitude is measured in a depth-uniform current. Hence, the first set of scales considers all interaction mechanisms involved while the Doppler effect is excluded using the second set of scales. If the Doppler effect dominates, the non-dimensional force/moment curves using the second set of scales are expected to collapse with each other.

Fig. 6 shows the variations of the horizontal force with kB for cases with and without the current using both sets of scales. The current velocity of $U = \pm 0.2$ m/s and $U = + 0.3$ m/s is considered. The non-dimensional force curves shown in Fig. 6 (a) almost collapse with each other, while the increase/decrease in the horizontal force is obvious in Fig. 6 (b) when the current-affected amplitude is used for the normalization. This indicates that the increase/decrease in the horizontal force due to the Doppler shifted effect is offset by other mechanisms; candidates include the generation of higher free harmonic waves and the drag force represented by the term $\rho U \partial\phi/\partial x$, an additional term introduced by the current in calculating the loads on the structure, see Eq. (A8) in the Appendix 2. These will be discussed in more detailed in the following sections.

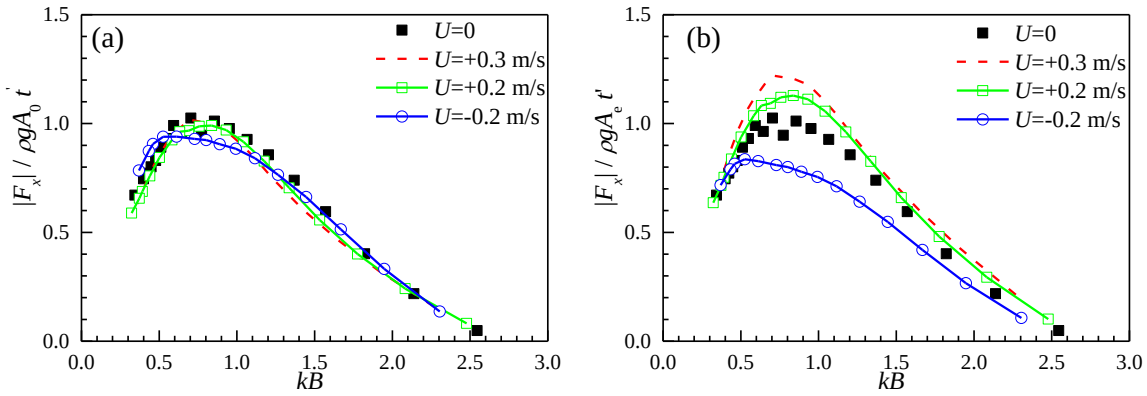

Fig. 6 Variations of the horizontal forces with the kB. (a) The horizontal force is non-dimensional dividing by $\rho g A_0 t'$; (b) the horizontal force is non-dimensional dividing by $\rho g A_e t'$.

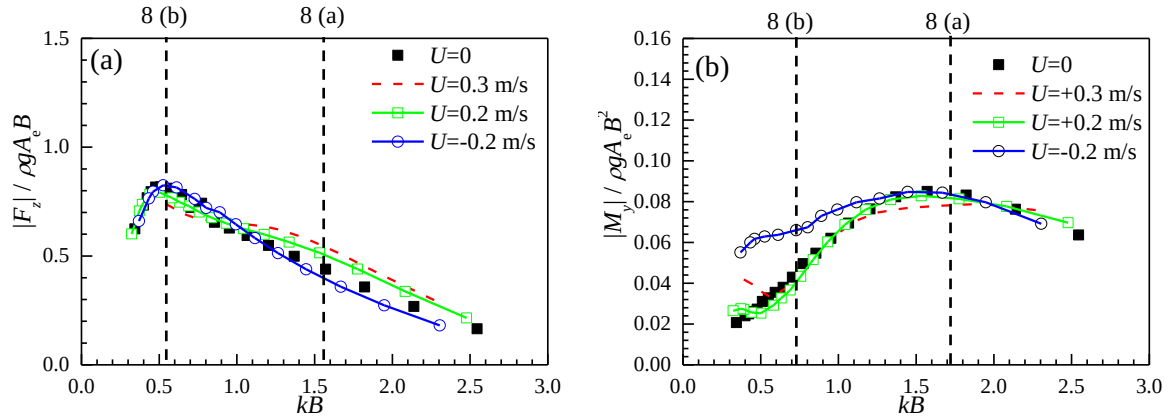

Fig. 7 Variations of the vertical force (a) and moment (b) with the kB.

The results for the vertical force and the moment are shown in Fig. 7 (a) and Fig. 7 (b), respectively. Only the results that are non-dimensinalized using the current-affected amplitude A_e are shown for brevity; the results considering the first set of scales are shown in Appendix 4. It can be seen that the curves for cases with and without currents are close with each other, although some differences are observed at certain wave numbers. The Doppler effect is found to dominate the vertical force and the moment on the submerged plate.

As mentioned previously, there are still some differences for the vertical forces for shorter waves ($kB > 1.27$ or $kh > 5$) and for the moment for longer waves ($kB < 1.27$ or $kh < 5$) even the second set of scales are used. This suggests that the incoming wave period/wavelength relative to the plate width is also an important parameter as expected to determine the behaviours of the interaction mechanism.

Pressure envelopes on the upper and lower surfaces of the submerged plate for the two representative waves, highlighted by the dashed lines in Fig.7, are shown in Fig. 8. The pressure is calculated by solving the Bernoulli's equation [42], hence, the total dynamic pressure is considered here; see also Eq. (A8). It can be seen that for a shorter wave ($kB = 1.57$ and $kh = 6.166$; Fig. 8(a)), the pressure on both the upper and lower surfaces increases in a following current while decreases in an opposing current. The results for wave-only cases sit in between. The pressure on the upper surface increases/decreases more than that on the lower surface in the following/opposing currents. This leads to a small increase/decrease in the vertical force at larger kB (or kh) as shown in Fig.7 (a). In addition, the pressure profiles on both lower and the upper surfaces are symmetric with respect to the centre of the plate for shorter waves. As the wave period increases (from $kB = 1.57$ to 0.53), the effect of the current are found to become less significant due to a decreasing U/C_{g0}, as shown in Fig. 8 (b). The pressure profiles on the upper surface become asymmetric with respect to the centre of the plate while the pressure profiles on the lower surface remain symmetric as the wave period increases. This explains the relatively larger difference in the moment at smaller kB (or kh), as shown in Fig. 7 (b).

The pressure behaviors at the edges of the plate shown in Fig. 8 may associate with the reflection characteristics at such locations. Patarapanich [12] and Lin et al. [64] found that the total reflections consist of reflections from edges and bottom of the plate. Maximum and minimum reflections occurred when the reflection components are in and out of phase with each other, respectively. For the testing condition shown in Fig. 8 (b), the interferences between the local flows and the plate are violent and may be in phase with each other, leading to maximum reflections hence maximum wave forces on the plate at this particular condition, as indicated in Fig. 6 and Fig. 7 (a). This explains the obvious increase in the pressure at the edges of the plate in Fig. 8 (b).

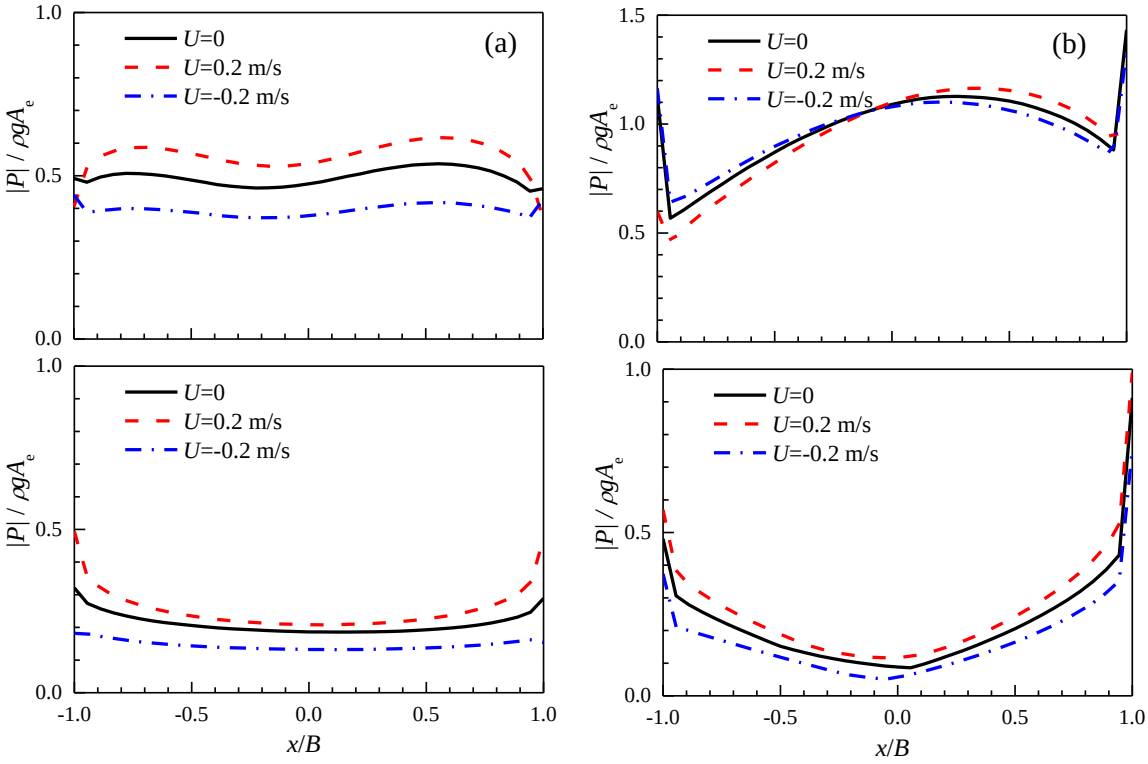

Fig. 8 The envelopes of the pressure on the upper (top) and lower (bottom) surfaces. (a) kB = 1.57 (kh = 6.166), U/C_{g0} = 0, ±0.18; (b) kB = 0.53 (kh = 2.095), U/C_{g0} = 0, ±0.10.

4.2 Generation of higher harmonic free waves

As discussed in Lin et al. [37], higher harmonics are generated as incoming waves approach the submerged plate and propagate over it due to a sudden change in the water depth. Part of these higher hamonics may be released as free waves during the propagation over the submerged plate. This section looks into how the interaction mechanism affect the generation of higher harmonic free waves, thus, on the wave-induced forces and moment on the submerged plate.

Time series and the corresponding spectra of the horizontal force on the submerged plate are shown in Fig. 9 for T = 2.0 s (kB = 0.77 and kh = 3.03). It can be seen that the linear horizontal forces for this particular wave increases in a following current and decreases in an opposing current. This is consistent with what has been observed in Fig. 6 (b). While the trend in the second order harmonic horizontal force is in contrast to that of linear components. The second order harmonics are observed to be ordered from the largest to the smallest in initial still water, on following and on opposing currents. The contributions from the second order harmonics are more than 25% of the total horizontal forces on the submerged plate. The increase/decrease in the linear components due to the presence of the following/opposing current may be compensated by the decrease/increase in the second order harmonic horizontal forces. Similar behaviours are found for the vertical forces and the moment, with relatively smaller contributions from higher harmonics. Hence, the solution for vertical force and the moment show certain consistencies with the Doppler shifted solutions as discussed previously. This is as expected as the generation of higher harmonic free waves is found to be more violent at edges of the submerged plate by which the horizontal force behaviour is dominated. In addition to the 2nd order sum term, i.e. 2nd order harmonics discussed previously, the nonlinear evolution of waves and combined wave-current flows also leads to the generation of 2nd order frequency difference term, i.e. wave component at f = 0 in Fig. 9, for all three flow configurations [28, 55]. Globally, this term would lead to non-zero temporal mean values in the pressure records (which are not shown here for brevity).

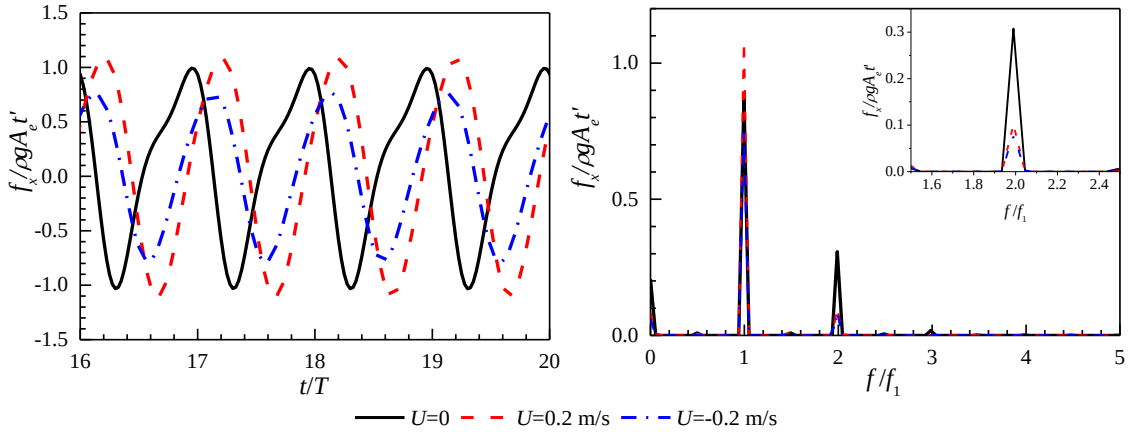

Fig. 9 Time series of the horizontal force on the submerged plate and the corresponding force spectra for cases with kh = 3.03 (kB = 0.77).

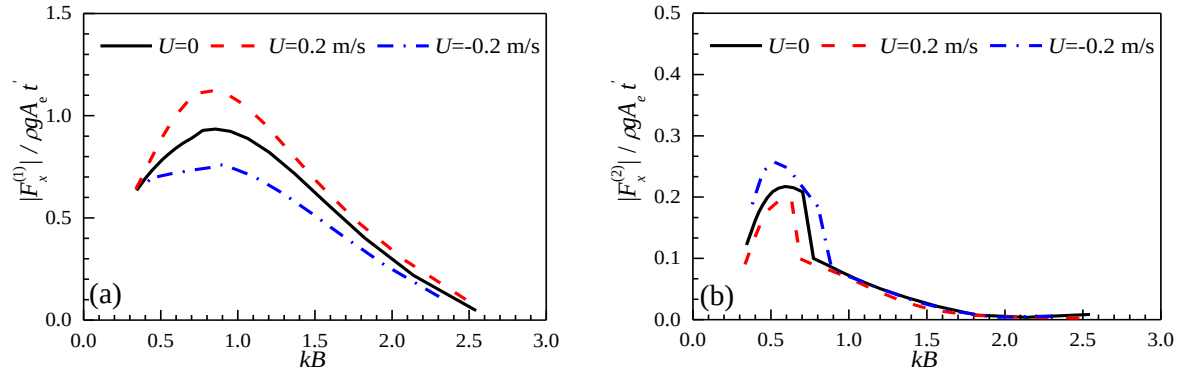

Fig. 10 Variations of the linear (a) and 2nd order (b) horizontal forces with the kB.

Variations of the linear and the 2nd order horizontal forces on the submerged plate with the kB are shown in Fig. 10. The higher order free waves are extracted from the linear components using a two-point method in [37]. Both the amplitudes and phases of the higher order free waves are determined (though the phases are not shown here for brevity). Details can be found in [37].

Stronger non-linear wave-structure interactions are observed in shallow water (i.e. low-frequency region) as expected. The contributions of the 2nd harmonics are up to 30% for kB < 1.28 (kh < 5). At relatively deep water (i.e. high-frequency region) with kB > 1.28 (kh > 5), the nonlinearity is weak, thus, the generated 2nd order harmonics are relatively small with a minimum value of about 1% of the corresponding linear component. It can be seen from Figs. 9-10 that the linear components for regular waves traveling on a following current are larger than those on an opposing current, and the results for wave-only cases sit in between for all waves considered. The 2nd order harmonics show opposite trends with the largest and smallest values observed in an opposing and following current, respectively. This confirms that the generation of higher harmonics needs to be considered for accurate estimation of the horizontal forces on a submerged plate in coastal areas where wave and current co-exists. The linear potential flow theory and the Doppler shifted solutions are no longer applicable. It is noted that the phase difference between the linear and higher harmonic free waves is also required for doing the addition properly, which is not shown here for brevity.

4.3 Current-induced drag force

The effect of current on wave loads is reflected in the form of 1) the velocity potential ϕ (hence nonlinear local wave fields) and 2) the drag force, represented by the term $\rho U \partial\phi/\partial x$; see also Eq. (A8)

in the Appendix 2. Rey and Touboul [35] suggested that the drag forces introduced by a following current may result in an increase in the pressure on the submerged plate, though details were not presented. This will be further explored in this section using NWTs, which cannot be easily achieved by physical experiments such as those in [35].

A new series of numerical simulations are carried out to investigate the effect of the current-induced drag force, hence the direct effect of current velocity on the total wave loads. In the new set of numerical simulations, the effect of 1) is considered by using the current-affected amplitude A_e and the current-affected wavelength, and the effect of 2) is excluded by setting the current velocity $U = 0$. We note that the effects of 1) and 2) are actually coupled together, thus, the physical processes described by the two sets of numerical simulations are not exactly the same, for example, the reflection and transmission behaviours of incoming waves may be different. Nevertheless, it is reasonable to assume that the contribution of the current-induced drag force would dominates the differences by applying this treatment. The tentative conclusions drawn are still helpful and of value.

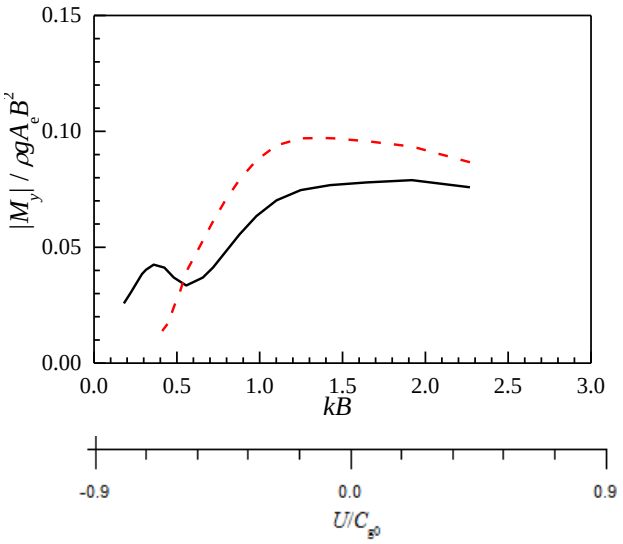

Fig. 11 Variations of the predicted moment by the present model on the submerged plate with the kB. The solid and dashed line shows the results with and without the term $\rho U \partial\phi/\partial x$.

The results from the two sets of numerical simulations in terms of the moment are summarized in Fig. 11. The combined effect of vertical and horizontal forces is reflected in the moment, hence, the individual behaviour of vertical and horizontal forces is omitted here for brevity. The equivalent abscissa in terms of U/C_{g0} is also shown for reference. It can be seen from the figure that for smaller kB (kh) the presence of the current-induced drag leads to an increase in the moment while as kB (kh) increases to kB > 0.51 (kh > 2), the moment on the submerged plate decreases with the term $\rho U \partial\phi/\partial x$, i.e. the current-induced drag force. The effect/behaviour of the drag force is coupled with the incoming wave periods and/or the current direction.

5. CONCLUSIONS

The NWTs based on potential flow theory are applied in this study to estimate the forces and the moment on a submerged plate induced by combined wave-current flows. The NWTs solve the Laplacian equation based on the higher order boundary element method (HOBEM). The free surface motion is tracked by the fourth-order Runge-Kutta (RK4) scheme. The capabilities of the NWTs in providing force predictions are verified by comparing with theoretical results and experimental measurements. The validated NWTs are then applied to perform an in-depth investigation on the interaction mechanisms involved.

The analysis shows that the horizontal and the vertical force, hence the moment, are affected in opposite way by the currents. This results from the combined effect of the Doppler shifted effect, the generation of higher harmonic waves and the current-induced drag force. The drag force is the additional advection term, $\rho U \partial\phi/\partial x$, in the pressure equation associated with the existence of a current. The Doppler shifted effect is found to dominate the vertical force and the moment on the plate. Whereas, the generation of higher harmonic waves is also found to have significant effect on the horizontal force. The contribution of the 2nd order harmonic waves is up to 30% of linear component for longer waves. This shows an effect opposite to the linear components, and the Doppler shifted solutions. For smaller kh at relatively low-frequency region, the presence of the drag force leads to an increase in the moment, while as kh increases ($kh > 2$ and $kB > 0.51$) the moment on the submerged plate decreases with the term $\rho U \partial\phi/\partial x$. The analysis/insights as such in this work would be useful and important to develop an efficient design tool that can be incorporated into the practical engineering process for submerged breakwaters in coastal areas.

It is noted that this work only considered regular wave, however, the same approach used in this work could be easily extended to irregular waves. The linear superimposition on the Fourier components that defined by the underlying wave spectrum may be considered as in [35]. The discrete energy spectra for both incident and reflected waves as well as the transmitted waves can be obtained following the method in [44]. Obviously, the computational effort would increase when considering spectral waves. Rey and Touboul [35] considered both regular and irregular wave in their experiments, and found that these two show the same trends in presence of a current. Hence, it is reasonable to assume that the conclusions in this work for regular waves could be generalized to irregular waves. However, more analyses are required before the conclusion is made. We leave this additional complication for future.

ACKNOWLEDGE

The authors would like to acknowledge the financial support from the National Key R&D Program of China (Grant No. 2016YFE0200100) and National Natural Science Foundation of China (Grant Nos. 51679036 and 51761135011).

REFERENCE

1. Yu, X., 2002. Functional performance of a submerged and essentially horizontal plate for offshore wave control: a review. Coastal engineering journal, 44(02), 127-147.
2. Liao, C., Tong, D. and Chen, L., 2018. Pore pressure distribution and momentary liquefaction in vicinity of impermeable slope-type breakwater head. Applied Ocean Research, 78, 290-306.
3. Liao, C., Tong, D., Jeng, D.S. and Zhao, H., 2018. Numerical study for wave-induced oscillatory pore pressures and liquefaction around impermeable slope breakwater heads. Ocean Engineering, 157, 364-375.
4. Morison, J.R., Johnson, J.W. and Schaaf, S.A., 1950. The force exerted by surface waves on piles. Journal of Petroleum Technology, 2(05), 149-154.
5. Kaplan, P., Murray, J.J. and Yu, W.C., 1995. Theoretical analysis of wave impact forces on platform deck structures. Pro. Int. Conf. on Offshore Mechanics and Arctic Engineering, OMAE '95. AMSE, 189-198.
6. Isaacson, M. and Bhat, S., 1996. Wave forces on a horizontal plate. International Journal of Offshore and Polar Engineering, 6(01), 19-26.
7. Bea, R.G., Xu, T., Stear, J. and Ramos, R., 1999. Wave forces on decks of offshore platforms. Journal of waterway, port, coastal, and ocean engineering, 125(3), 136-144.
8. Allsop, N.W.H., Cuomo, G., and Tirindelli, M., 2006. New prediction method for wave-in-deck loads on exposed piers/jetties/bridges. Proc. 30th International Conference Coastal Engineering 2006, 5, 4482-4493.
9. Cuomo, G., Tirindelli, M. and Allsop, W., 2007. Wave-in-deck loads on exposed jetties. Coastal Engineering, 54(9), 657-679.

10. Siew, P.F., Hurley D.G., 1977. Long surface waves incident on a submerged horizontal plate. J Fluid Mech. 83, 141.
11. Vada, T., 1987. A numerical solution of the second-order wave-diffraction problem for a submerged cylinder of arbitrary shape. J Fluid Mech 174, 23.
12. Patarapanich, M., 1984. Forces and moment on a horizontal plate due to wave scattering. Coast Eng. 8, 279–301.
13. An, S. and Faltinsen, O.M., 2012. Linear free-surface effects on a horizontally submerged and perforated 2D thin plate in finite and infinite water depths. Applied Ocean Research, 37, 220-234.
14. Guo, A., Fang, Q. and Li, H., 2015. Analytical solution of hurricane wave forces acting on submerged bridge decks. Ocean Engineering, 108, 519-528.
15. Koo, W., Kim, M.H., Tavassoli, A. 2004. Fully nonlinear wave-body interactions with fully submerged dual cylinders. Int. J. Offshore Polar Eng. 14 (3). Paper No. ISOPE-04-14-3-210.
16. Abbasnia, A., Ghiasi, M., 2013. A fully nonlinear wave interaction with an array of submerged cylinders by NURBS numerical wave tank and acceleration potential. Ships Offshore Struct. 9, 404-417.
17. Bai, W., Hannan, M.A., Ang, K.K., 2014. Numerical simulation of fully nonlinear wave interaction with submerged structures: Fixed or subjected to constrained motion. J. Fluids Struct. 49, 534–553.
18. Guerber, E., Benoit, M., Grilli, S.T. and Buvat, C., 2012. A fully nonlinear implicit model for wave interactions with submerged structures in forced or free motion. Engineering Analysis with Boundary Elements, 36(7), 1151-1163.
19. Dong, J., Wang, B. and Liu, H., 2016. Wave forces on a submerged horizontal plate over a sloping beach due to a solitary wave. In 12th ISOPE Pacific/Asia Offshore Mechanics Symposium. International Society of Offshore and Polar Engineers.
20. Seiffert, B., Hayatdavoodi, M. and Ertekin, R.C., 2014. Experiments and computations of solitary-wave forces on a coastal-bridge deck. Part I: Flat plate. Coastal Engineering, 88, 194-209.
21. Hayatdavoodi, M., Seiffert, B. and Ertekin, R.C., 2015. Experiments and calculations of cnoidal wave loads on a flat plate in shallow-water. Journal of Ocean Engineering and Marine Energy, 1(1), 77-99.
22. Zhao, B.B., Duan, W.Y. and Ertekin, R.C., 2014. Application of higher-level GN theory to some wave transformation problems. Coastal Engineering, 83, 177-189.
23. Zhao, B.B., Ertekin, R.C., Duan, W.Y. and Hayatdavoodi, M., 2014. On the steady solitary-wave solution of the Green–Naghdi equations of different levels. Wave Motion, 51(8), 1382-1395.
24. Zhao, B.B., Duan, W.Y., Ertekin, R.C. and Hayatdavoodi, M., 2015. High-level Green–Naghdi wave models for nonlinear wave transformation in three dimensions. Journal of Ocean Engineering and Marine Energy, 1(2), 121-132.
25. Chakrabarti, S.K., 1996. Shear current and its effect on fixed and floating structures. Adv. Coas. Ocean Eng., 2, 231-276.
26. Stacey, M.T., Monismith, S.G., Buran, J.R., 1999. Measurements of Reynolds stress profiles in unstratified tidal flow. J. Geophys. Res., 104, 10935-10949.
27. Gunn, K., Stock-Williams, C., 2013. On validating numerical hydrodynamic models of complex tidal flow. Inter. J. Mar. Energy, 3, e82-e89.
28. Chen, L.F., Stagonas, D., Santo, H., Buldakov, E.V., Simons, R.R., Taylor, P.H. and Zang, J., 2019. Numerical modelling of interactions of waves and sheared currents with a surface piercing vertical cylinder. Coastal Engineering, 145, 65-83.
29. Lavrenov, I., 2013. Wind-waves in oceans: dynamics and numerical simulations. Springer Science & Business Media.
30. Hedges, T.S. and Lee, B.W., 1992. The equivalent uniform current in wave-current computations. Coastal engineering, 16(3), 301-311.
31. Grue, J. and Palm, E., 1985. Wave radiation and wave diffraction from a submerged body in a uniform current. Journal of Fluid Mechanics, 151, 257-278.
32. Nossen, J., Grue, J. and Palm, E., 1991. Wave forces on three-dimensional floating bodies with small forward speed. Journal of Fluid Mechanics, 227, 135-160.
33. Rey, V., Capobianco, R. and Dulou, C., 2002. Wave scattering by a submerged plate in presence of a steady uniform current. Coastal Engineering, 47(1), 27-34.
34. Zhang, J.S., Zhang, Y., Jeng, D.S., Liu, P.F. and Zhang, C., 2014. Numerical simulation of wave–

current interaction using a RANS solver. Ocean Engineering, 75, 157-164.
35. Rey, V. and Touboul, J., 2011. Forces and moment on a horizontal plate due to regular and irregular waves in the presence of current. Applied Ocean Research, 33(2), 88-99.
36. Cheng, Y., Ji, C., Ma, Z., Zhai, G. and Oleg, G., 2017. Numerical and experimental investigation of nonlinear focused waves-current interaction with a submerged plate. Ocean Engineering, 135, 11-27.
37. Lin, H., Ning, D., Zou, Q., Teng, B., Chen, L., 2009. Current effects on nonlinear wave scattering by a submerged plate. J Waterw Port, Coastal, Ocean Eng. 1-12.
38. Koo, W., Kim, M.H., 2007. Current effects on nonlinear wave-body interactions by a 2D fully nonlinear numerical wave tank. J Waterw Port, Coastal, Ocean Eng. 133, 136-146.
39. Liu, C., Huang, Z., Keat Tan, S., 2009. Nonlinear scattering of non-breaking waves by a submerged horizontal plate: Experiments and simulations. Ocean Eng. 36, 1332–1345.
40. Baddour, R.E., and Song, S.W., 1990. Interaction of higher-order water waves with uniform currents. Ocean Eng. 17, 551–568.
41. Bai, W., Eatock Taylor, R., 2006. Higher-order boundary element simulation of fully nonlinear wave radiation by oscillating vertical cylinders. Appl Ocean Res. 28, 247–265.
42. Ning, D., Wang, R., Chen, L., Li, J., Zang, J., Cheng, L., Liu, S.X., 2017. Extreme wave run-up and pressure on a vertical seawall. Appl Ocean Res 67, 188-200.
43. Li, F.C., Ting, C.L., 2012. Separation of free and bound harmonics in waves. Coast Eng. 67, 29–40.
44. Drevard, D., Rey, V. and Fraunié, P., 2009. Partially standing wave measurement in the presence of steady current by use of coincident velocity and/or pressure data. Coastal Engineering, 56(9), 992-1001.
45. Yu, X., 2002. Functional performance of a submerged and essentially horizontal plate for offshore wave control: a review. Coastal engineering journal, 44(02), 127-147.
46. Liao, C., Tong, D. and Chen, L., 2018. Pore pressure distribution and momentary liquefaction in vicinity of impermeable slope-type breakwater head. Applied Ocean Research, 78, 290-306.
47. Liao, C., Tong, D., Jeng, D.S. and Zhao, H., 2018. Numerical study for wave-induced oscillatory pore pressures and liquefaction around impermeable slope breakwater heads. Ocean Engineering, 157, 364-375.
48. Toffoli, A., Cavaleri, L., Babanin, A.V., Benoit, M., Bitner-Gregersen, E.M., Monbaliu, J., Onorato, M., Osborne, A.R. and Stansberg, C.T., 2011. Occurrence of extreme waves in three-dimensional mechanically generated wave fields propagating over an oblique current. Natural Hazards and Earth System Sciences, 11(3), 895-903.
49. Toffoli, A., Waseda, T., Houtani, H., Kinoshita, T., Collins, K., Proment, D. and Onorato, M., 2013. The excitation of rogue waves in a variable medium: An experimental study on the interaction of water waves and currents. Physical Review E, 87(5), 051201.
50. Toffoli, A., Waseda, T., Houtani, H., Cavaleri, L., Greaves, D. and Onorato, M., 2015. Rogue waves in opposing currents: an experimental study on deterministic and stochastic wave trains. Journal of Fluid Mechanics, 769, 277-297.
51. Onorato, M., Proment, D. and Toffoli, A., 2011. Triggering rogue waves in opposing currents. Physical review letters, 107(18), 184502.
52. Alberello, A., Chabchoub, A., Monty, J.P., Nelli, F., Lee, J.H., Elsnab, J. and Toffoli, A., 2018. An experimental comparison of velocities underneath focussed breaking waves. Ocean Engineering, 155, 201-210.
53. Bretherton, F.P. and Garrett, C.J.R., 1968. Wavetrains in inhomogeneous moving media. Proceedings of the Royal Society of London. Series A. Mathematical and Physical Sciences, 302(1471), 529-554.
54. Chen, L.F., Ning, D.Z., Teng, B. and Zhao, M., 2017. Numerical and experimental investigation of nonlinear wave-current propagation over a submerged breakwater. Journal of Engineering Mechanics, 143(9), p.04017061.
55. Chen, L.F., Zang, J., Hillis, A.J., Morgan, G.C.J. and Plummer, A.R., 2014. Numerical investigation of wave–structure interaction using OpenFOAM. Ocean Engineering, 88, 91-109.
56. Ning, D.Z., Wang, R.Q., Chen, L.F. and Sun, K., 2019. Experimental investigation of a land-based dual-chamber OWC wave energy converter. Renewable and Sustainable Energy Reviews, 105, 48-

60.
57. Chen, L., Taylor, P.H., Draper, S. and Wolgamot, H., 2019. 3-D numerical modelling of greenwater loading on fixed ship-shaped FPSOs. Journal of Fluids and Structures, 84, 283-301.
58. Ning, D.Z., Zang, J., Liu, S.X., Taylor, R.E., Teng, B. and Taylor, P.H., 2009. Free-surface evolution and wave kinematics for nonlinear uni-directional focused wave groups. Ocean Engineering, 36 (15-16), 1226-1243.
59. Nelli, F., Bennetts, L.G., Skene, D.M., Monty, J.P., Lee, J.H., Meylan, M.H. and Toffoli, A., 2017. Reflection and transmission of regular water waves by a thin, floating plate. Wave Motion, 70, 209-221.
60. Skene, D.M., Bennetts, L.G., Meylan, M.H. and Toffoli, A., 2015. Modelling water wave overwash of a thin floating plate. Journal of Fluid Mechanics, 777.
61. Greco, M., 2001. A Two-dimensional Study of Green-Water Loading (Doctoral dissertation, Norwegian University of Science and Technology).
62. Zhou, B.Z., Ning, D.Z., Teng, B. and Bai, W., 2013. Numerical investigation of wave radiation by a vertical cylinder using a fully nonlinear HOBEM. Ocean Engineering, 70,1-13.
63. Ning, D.Z., Wang, R.Q., Gou, Y., Zhao, M. and Teng, B., 2016. Numerical and experimental investigation of wave dynamics on a land-fixed OWC device. Energy, 115, 326-337.
64. Lin, H.X., Ning, D.Z., Zou, Q.P., Teng, B. and Chen, L.F., 2014. Current effects on nonlinear wave scattering by a submerged plate. Journal of Waterway, Port, Coastal, and Ocean Engineering, 140(5), p.04014016.
65. Huseby, M. and Grue, J., 2000. An experimental investigation of higher-harmonic wave forces on a vertical cylinder. Journal of Fluid Mechanics, 414, 75-103.
66. Zou, Q. and Peng, Z., 2011. Evolution of wave shape over a low-crested structure. Coastal Engineering, 58(6), .478-488.
67. Peng, Z., Zou, Q., Reeve, D. and Wang, B., 2009. Parameterisation and transformation of wave asymmetries over a low-crested breakwater. Coastal engineering, 56(11-12), .1123-1132.
68. Chen, H. and Zou, Q., 2019. Effects of following and opposing vertical current shear on nonlinear wave interactions. Applied Ocean Research, 89, .23-35.

Appendix 1 Underlying numerical methods of the fully NWTs

The sketch of the problem considered in this study can be seen in Fig. 1. A Cartesian coordinate system *Oxz* is introduced: the *x*-axis is positive in the wave propagation direction with its origin at the left end of the tank, and the *z*-axis is positive upward with $z = 0$ at the mean free surface, as shown in Fig. 1.

In the NWTs that based on potential flow theory, the fluid motions are described by the velocity potential that satisfies Laplace equation within the computation domain, assuming that the flow considered is inviscid, incompressible and irrotational. In the presence of currents, the total velocity potential within the domain is given by $\Phi = Ux + \phi$ where ϕ is the perturbation velocity potential induced by waves, and U is the velocity of a constant current propagating in parallel with the incoming wave.

Both the fully nonlinear kinematic and dynamic boundary conditions are satisfied on the instantaneous free surface (Γ_F, Fig. 1) for the description of the free surface dynamics. Extra damping terms are incorporated in the original free surface boundary conditions to act as numerical beaches at both ends of the NWT. The bottom (Γ_B, Fig. 1), right end of the NWT (Γ_O, Fig. 1) and the structure (Γ_S, Fig. 1) are considered impermeable i.e. the normal velocities at these boundaries are set to zero. The combined wave-current flows are generated from the left end of the NWT (Γ_I, Fig. 1) by prescribing fluid particle velocity from the 2nd order Stokes wave theory at the input boundary faces (Γ_I, Fig. 1).

The boundary value problem (BVP) of wave-current-structure interactions in terms of the total velocity potential Φ can then be described mathematically as,

667
$$\begin{cases} \nabla^2\Phi = 0;\ \Phi = Ux + \phi \quad \text{within } \Omega \\ \dfrac{\partial \eta}{\partial t} = \dfrac{\partial \Phi}{\partial z} - \Phi_x \eta_x - \Phi_y \eta_y - \nu_1(x)(\eta - \eta_e) - \nu_2(x)\eta \quad \text{on } \Gamma_{\mathrm{F}} \\ \dfrac{\partial \Phi}{\partial t} = -g\eta - \dfrac{1}{2}|\nabla\Phi|^2 - \nu_1(x)(\Phi - \Phi_e) - \nu_2(x)\Phi \quad \text{on } \Gamma_{\mathrm{F}} \\ \dfrac{\partial \Phi}{\partial n} = 0 \ \text{ on } \Gamma_{\mathrm{B}}, \Gamma_{\mathrm{O}}, \Gamma_{\mathrm{S}};\ \ \dfrac{\partial \Phi}{\partial n} = -\dfrac{\partial \Phi_I}{\partial x} \ \text{ on } \Gamma_{\mathrm{I}} \end{cases} \tag{A1}$$

668 Eq. (A1) is re-written in terms of U and ϕ,

669
$$\begin{cases} \nabla^2\phi = 0 \quad \text{within } \Omega \\ \dfrac{\partial \eta}{\partial t} = \dfrac{\partial \phi}{\partial z} - \phi_x \eta_x - \phi_y \eta_y - U\dfrac{\partial \eta}{\partial x} - \nu_1(x)(\eta - \eta_e) - \nu_2(x)\eta \quad \text{on } \Gamma_{\mathrm{F}} \\ \dfrac{\partial \phi}{\partial t} = -g\eta - \dfrac{1}{2}|\nabla\phi|^2 - U\dfrac{\partial \phi}{\partial x} - \dfrac{1}{2}U^2 - \nu_1(x)(\phi - \phi_e) - \nu_2(x)\phi \quad \text{on } \Gamma_{\mathrm{F}} \\ \dfrac{\partial \phi}{\partial n} = 0 \ \text{ on } \Gamma_{\mathrm{B}}, \Gamma_{\mathrm{O}}, \Gamma_{\mathrm{S}};\ \ \dfrac{\partial \phi}{\partial n} = -\dfrac{\partial \phi_I}{\partial x} \ \text{ on } \Gamma_{\mathrm{I}} \end{cases} \tag{A2}$$

670 The BVP for wave-current-structure interactions can then be transformed to Eq. (A3) by introducing
671 the material derivatives D/Dt,

672
$$\begin{cases} \nabla^2\phi = 0 \quad \text{within } \Omega \\ \dfrac{D\eta}{Dt} = \dfrac{\partial \phi}{\partial z} - \nu_1(x)(\eta - \eta_e) - \nu_2(x)\eta \quad \text{on } \Gamma_{\mathrm{F}} \\ \dfrac{D\phi}{Dt} = -g\eta + \dfrac{1}{2}|\nabla\phi|^2 - \nu_1(x)(\phi - \phi_e) - \nu_2(x)\phi \quad \text{on } \Gamma_{\mathrm{F}} \\ \dfrac{\partial \phi}{\partial n} = 0 \ \text{ on } \Gamma_{\mathrm{B}}, \Gamma_{\mathrm{O}}, \Gamma_{\mathrm{S}};\ \ \dfrac{\partial \phi}{\partial n} = -\dfrac{\partial \phi_I}{\partial x} \ \text{ on } \Gamma_{\mathrm{I}} \end{cases} \tag{A3}$$

673 in which $D/Dt = \partial/\partial t + v\cdot\nabla = \partial/\partial t + \nabla\Phi\cdot\nabla$, i.e. $v = \nabla\Phi = U\mathbf{i} + \nabla\phi$. η is the free surface elevation, t the
674 time, x the horizontal distance away from the inlet boundary (Γ_{I}). η_e and ϕ_e are the free surface elevation
675 and the velocity potential aiming to achieve within the damping zones, respectively. These are
676 determined by the numerical simulations without the structure in place, i.e. the values measured in the
677 absence of the obstacle under the same computational conditions when there are structures.

678 The incident velocity ϕ_I is given based on the 2nd order analytical solution in this study [40],

679
$$\begin{aligned} \phi_I = {} & \frac{gA_e}{\omega - kU}\frac{\cosh k(z+h)}{\cosh kh}\sin(kx - \omega t) \\ & + \frac{3}{8}A_e^2(\omega - kU)\frac{\cosh 2k(z+h)}{\sinh^4 kh}\sin 2(kx - \omega t) \end{aligned} \tag{A4}$$

680 in which A_{e} is the current-affected wave amplitude. Based on the conservation of wave action [53], A_{e}
681 satisfies the following relation:

682
$$A_e = A_0\sqrt{\frac{\omega - kU}{\omega}\frac{C_{g0}}{C_g}} \tag{A5}$$

683 where C_{g} is the group velocity, and A_0 and C_{g0} are the wave amplitude and the group velocity in the
684 absence of current, respectively. The wave number k satisfies the modified dispersion relation (ω -
685 $kU)^2 = gk\tanh kh$.

686 $v_1(x)$ and $v_2(x)$ are the damping parameters that increase from 0 to α_d gradually within the damping
687 zones. $\alpha_d = 1.0$ is the empirical artificial damping coefficient,

688 $$v_i(x) = \begin{cases} \alpha_d \omega (\frac{x - x_i}{L_b})^2 & (x < x_1 \text{ for } i = 1;\ x > x_2 \text{ for } i = 2) \\ 0 \end{cases} \quad \text{(A6)}$$

689 where ω is the angular frequency, x_1 and x_2 the starting positions of damping zones 1 and 2, respectively.
690 L_b is the length of the damping zone, which is twice the incident wavelength in this study.

691 The BVP in Eq. (A3) can be transformed into an integral equation,

692 $$\alpha(p)\phi(p) = \int_{\Gamma} (\phi(p) \frac{\partial G(q, p)}{\partial n} - G(q, p) \frac{\partial \phi(q)}{\partial n}) d\Gamma, \quad p \in \Gamma \quad \text{(A7)}$$

693 where p and q are the source and field points, respectively. α is the solid angle coefficient associated
694 with the surface geometry of a source point position, and $\Gamma = \Gamma_I + \Gamma_O + \Gamma_F + \Gamma_S$. Note that the bottom of
695 the NWT (Γ_B), is excluded due to the addition of the mirror image of the Rankine source about the
696 seabed. The Green function $G(p,q) = (\ln r_1 + \ln r_2)/2\pi$, where r_1 is the distance between the field point
697 and the source point, and r_2 is the distance between the field point and the image of the source point
698 about the bottom.

699 The integral equation (A7) is solved by the higher order boundary element method (HOBEM) in
700 which the boundary Γ is divided into a number of isoparametric elements. The geometric and physical
701 variables of isoparametric boundary elements are represented using the same quadratic shape functions.
702 A set of linear algebraic equations are then obtained by assembling the equation for each node on the
703 whole boundary Γ at each time step [41]. The preconditioned generalized conjugate residual (GCR)
704 method is used with a residual of 10^{-4} to solve the resulting set of linear algebraic equations. The fourth-
705 order Runge-Kutta (RK4) scheme is applied to advance the free surface from the initial calm conditions
706 to the time instant of interest.

707

708 **Appendix 2 Forces and moment on the structure**

709 The acceleration potential method is used for calculating the time derivation of the velocity potential
710 ϕ_t in order to obtain the wave pressure on the structure by solving the Bernoulli's equation [42]. The
711 total hydrodynamic wave forces and moment on the submerged plate are then calculated through the
712 integral of the pressure,

713 $$\begin{cases} F_x = -\rho \int_{\Gamma_B} (\frac{\partial \phi}{\partial t} + \frac{1}{2} |\nabla \phi|^2 + U \frac{\partial \phi}{\partial x}) n_x d\Gamma \\ F_z = -\rho \int_{\Gamma_B} (\frac{\partial \phi}{\partial t} + \frac{1}{2} |\nabla \phi|^2 + U \frac{\partial \phi}{\partial x}) n_z d\Gamma \\ M_y = -\rho \int_{\Gamma_B} (\frac{\partial \phi}{\partial t} + \frac{1}{2} |\nabla \phi|^2 + U \frac{\partial \phi}{\partial x}) (n_x (z - z_0) - n_z (x - x_0)) d\Gamma \end{cases} \quad \text{(A8)}$$

714 where n_x and n_z are the normal vectors, and (x_0, z_0) is the assumed rotation centre of the plate. It can
715 be seen from Eq. (A8) that the effect on the current on load values is reflected in the form of the velocity
716 potential ϕ, hence, nonlinear wave fields (the first two terms on the left hand side), and the drag force,
717 the last term in Eq. (A8).

718

719 **Appendix 3 Comparisons with the results in [35] for wave-only cases.**

720

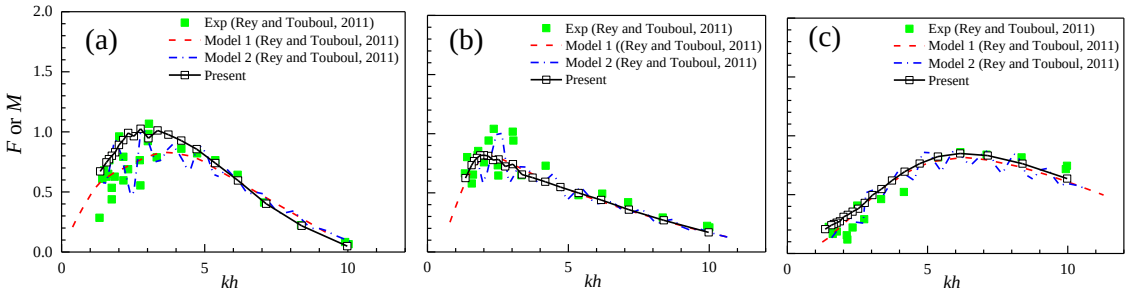

Fig. A3 Variations of the horizontal force $|F_x|/\rho g A_e t'$ (a), vertical force $|F_z|/\rho g A_e B$ (b), and moment $|M_y|/\rho g A_e B^2$ (c) with *kh* for wave-only casess. The moment is scaled up by a factor of 10.

Fig. A3 shows the variations of the forces and moment against the wave number *kh* for wave-only cases presented in [35]. The same trends as those in Fig. 5 for wave-current cases are observed. That is, the forces (a-b) incease with an increase in *kh* to their maximum, and then decrease with further increase of *kh*. The trend in moment is similar, and its behaviour in lower *kh* is less complex when compared to that in Fig. 5 (c) for wave-current cases. For higher *kh*, the behaviour of the moment is still affected by the wave period, i.e. *kh*. The force results are contaminated by the wave reflection more significantly when compared to the moment, hence the NWT results agree better with the experimental results in terms of moment, as expected. Not surprisingly, the analytical solutions in [35] that considered the wave reflections agree better with measured forces. In theory, the wave reflections can also be simulated using the NWTs, however, the detailed characteristics of the wave absorber were not provided in [35], hence omitted in this study.

Appendix 4 Variations of the vertical force and moment using the first set of scales

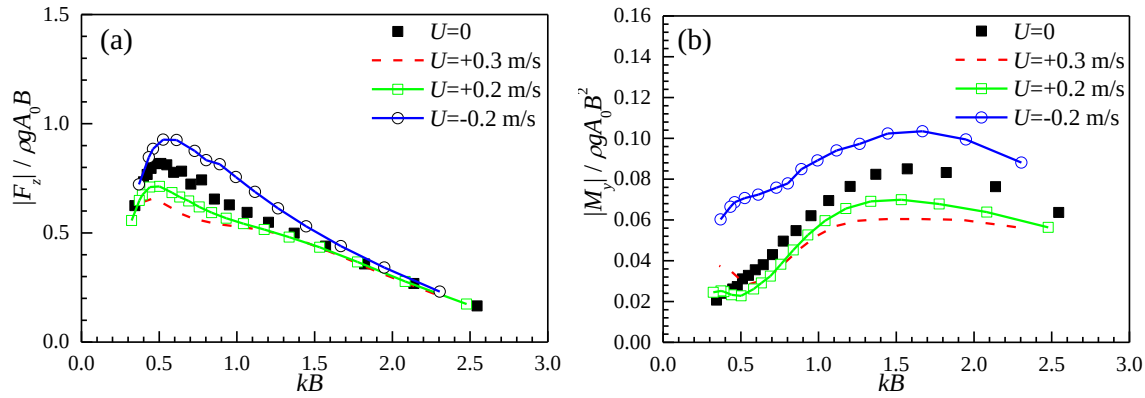

Fig. A4 Variations of the vertical force (a) and moment (b) with *kB*. The first set of scales, considering the nominal wave amplitude A_0, are used.

The effect of a depth-uniform current on the vertical force and moment on the submerged plate is studied in Fig. A4 using the first set of scales, i.e. the nominal wave amplitudes measured in still water are considered. It can be seen that both the vertical force and moment increase in an opposing current, and decrease in a following current. This is consistent with Doppler shifted solutions, indicating that the Doppler shifted effect dominate both the vertical force and moment on the submerged plate.